Compressive Sensing Hyperspectral Imager in the LWIR for Chemical Plume Detection

Stephanie M. Craig*[a], Julia R. Dupuis[a], John P. Dixon[a], Martín Anguita[a], David Mansur[a], S. Chase Buchanan[a], Eric R. Kehoe[b], Chris Peterson[b], Louis Scharf[b], Michael M. Kirby[b]

[a]Physical Science Inc., 20 New England Business Center, Andover, MA 01810
Tel: 978-689-0003; Fax: 978-689-3232; www.psicorp.com
[b]Dept. of Mathematics, Colorado State University, 841 Oval Drive, Fort Collins, CO 80523

ABSTRACT

An environmentally hardened compressive sensing hyperspectral imager (CS-HSI) operating in the long wave infrared (LWIR) has been developed for low-cost, standoff, wide area early warning of chemical vapor plumes. The CS-HSI employs a single-pixel architecture achieving an order of magnitude cost reduction relative to conventional HSI systems and a favorable pixel fill factor for standoff chemical plume imaging. A low-cost digital micromirror device modified for use in the LWIR is used to spatially encode the image of the scene; a Fabry-Perot tunable filter in conjunction with a single element mercury cadmium telluride photo-detector is used to spectrally resolve the spatially compressed data. A CS processing module reconstructs the spatially compressed spectral data, where both the measurement and sparsity basis functions are tailored to the CS-HSI hardware and chemical plume imaging. An automated target recognition algorithm is applied to the reconstructed hyperspectral data employing a variant of the adaptive cosine estimator for detection of chemical plumes in cluttered and dynamic backgrounds. The approach also offers the capability to generate detection products in compressed space with no CS reconstruction. This detection in transform space can be performed with a computationally lighter minimum variance distortionless response algorithm, resulting in a bandwidth advantage that supports efficient search and confirm modes of operation.

The development, characterization, and a series of capability demonstrations of an advanced prototype CS-HSI sensor are presented. Capability demonstrations include chemical plume imaging and detection of R-134 at mission-relevant concentration pathlength levels in laboratory and operationally relevant settings at 90% compression.

Keywords: Compressive sensing, longwave infrared, hyperspectral imaging sensor, digital micromirror device, chemical plume imaging, standoff early warning detection

1. TECHNOLOGY OVERVIEW

Physical Sciences Inc. and Colorado State University developed an environmentally hardened compressive sensing hyperspectral imager (CS-HSI) operating in the longwave infrared (LWIR) spectral range for low-cost, wide area early warning of chemical vapor plumes at standoffs of 3 km. The CS application drives a single pixel architecture for the CS-HSI sensor which eliminates the requirement for commonly used high-cost, mechanically cooled focal plane arrays in traditional LWIR HSI sensors. Furthermore, this sensor presents a disruptive technology to these traditional chemical sensors with respect to projected unit price (~$50k) and form factor, and enables widespread deployment over a host of standoff detection applications. A secondary benefit of this capability is intelligent data bandwidth management realized through use of optimized measurement and sparsity bases for chemical plume imaging, enabling low-data bandwidth communications. Detection has also been shown to be effective in compressed space, representing an additional bandwidth benefit. The key components of the CS-HSI are:

- A low-cost digital micromirror device (DMD) to spatially encode an image of the scene,

* Corresponding author: scraig@psicorp.com

- An LWIR Fabry-Perot tunable filter (FPTF) employing a mercury cadmium telluride (MCT) single element photodetector (PD) to spectrally resolve the spatially integrated image while mitigating background instrument radiance,
- A CS processing module to reconstruct the spatially compressed hyperspectral image where the measurement basis functions are specifically tailored to the CS-HSI hardware and chemical plume imaging,
- An automated target recognition (ATR) algorithm module employing a variant of the adaptive cosine estimator (ACE) and minimum variance distortionless response (MVDR) for detection of the chemical plumes in cluttered and dynamic backgrounds, and
- A hardened, waterproof housing for the sensor, supporting outdoor field testing with an IP65 rating

Figures 1a and 1b illustrate the CS-HSI concept, which has been reported on previously. [1] Light from the scene passes through the FPTF module, which provides spectral resolution to the acquired data. The FPTF is located at the entrance pupil of the system, which forces a reduced background in the out-of-band energy due to the Narcissus effect. An image of the scene is formed on the DMD, which spatially encodes that image using an optimally ordered Walsh Hadamard (WH) measurement basis. The DMD is modulated at 11.3 kHz enabling background rejection between energy from the scene and that from inside the instrument. The spatially encoded light is then focused onto a single element MCT PD where the intermediate data product recorded is a series of N, WH mask-scene dot products for each wavelength. The output of the CS-HSI is a series of N×M detector voltages where N is the number of WH masks and M is the number of wavelengths sampled by the FPTF. These voltages are either used with the CS module to reconstruct a hyperspectral data cube for ATR detection algorithms or be used directly for detection in compressed space. The single pixel imagery is reconstructed into 64×64 pixel spatial format, implying that a maximum of 4096 binary WH masks can be used to image scene. However, a smaller fraction of these WH masks can be used, which achieves the compression for the CS-HSI sensor and results in faster data acquisition times. This is further explored in Section 2.2. Figure 1c shows a photograph of the CS-HSI in its environmentally hardened housing.

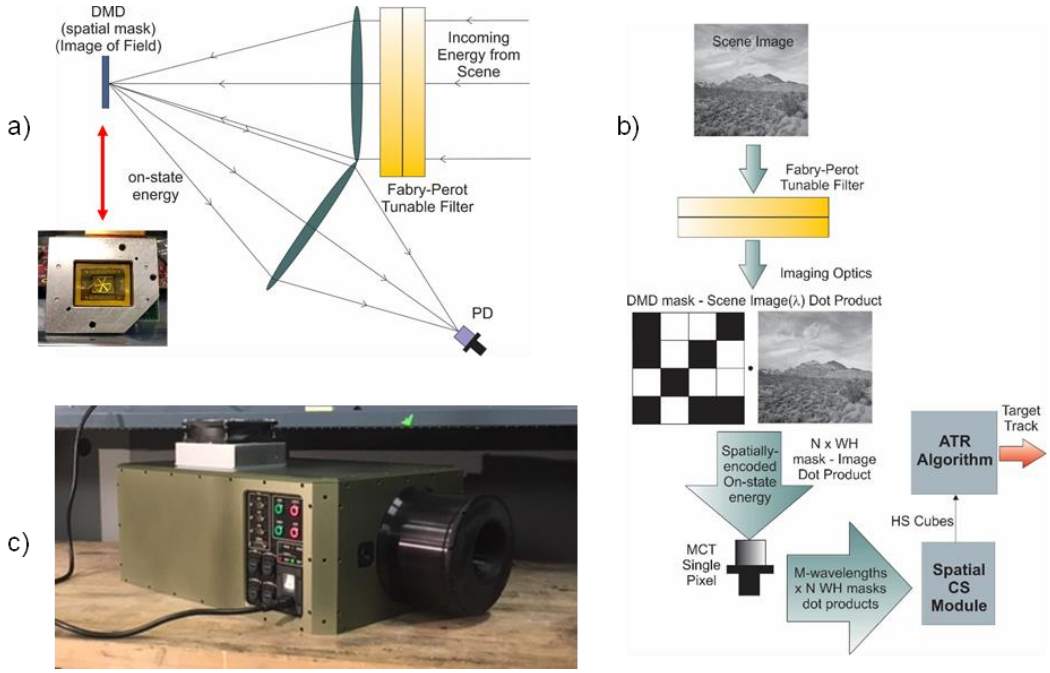

Figure 1. a) CS-HSI configuration, b) the associated data flow for the CS-HSI and c) photograph of the environmentally hardened CS-HSI.

Table 1 lists the threshold and objective Key Performance Parameters (KPPs) for the CS-HSI which have been derived from Joint Project Manager for NBC Contamination Avoidance Performance Specification for Commercial JSLSCAD document [2] coupled with the customer's goals for system price as embodied in the original acquisition target price

for JSLSCAD. Targets of interest include chemical warfare agents (CWAs), toxic industrial chemicals (TICs), and simulants. Threshold standoff range and probability of detection (P_d) is consistent with "ideal battlespace conditions", while the objective standoff and P_d requirement for ground mobile operation is consistent with "any battlespace/ environment condition". Fields of regard are based plume mapping in the direction of advance. The price specification is based on the JSLSCAD acquisition history, which had projected procurement of over 1800 units for a unit price of $100,000; the actual procurement fell to approximately 400 units at the actual unit price of approximately $450,000. The unit price of $100,000 is considered to be a threshold level for multiple 100 unit procurement. The objective of the CS-HSI system is to simultaneously meet JSLSCAD performance and cost targets.

Table 1. Threshold and objective capability derived KPPs for the CS-HSI.

KPP	Threshold [Objective]
Deployment capability	Stationary [Stationary/Ground Mobile]
Stand-off range	3 km [5 km / 2 km]
Vehicle speed	Stationary [35 mph]
Targets	CWAs, TICs, simulants
Interferents	Smoke, oil/fuel vapor/exhaust, dust
CL_{min} at 3 K ΔT	135 mg/m^2 [14 mg/m^2]
P_d	> 90% [> 90% / > 65%]
MTBFA	50 hours
Field of regard	60° AZ x 30° EL [120° AZ x 30° EL]
Cloud bearing accuracy	± 2°
Detection time	90 s [30 s]
Weight	50 lbs [25 lb]
Power	120 VAC 60 Hz [28 V]
Unit price in volume (100 units)	≤ $100,000 [≤ $50,000]

The following discussion details the sensor and housing designs, the system model, functional testing of the sensor, and the results of CS-HSI tests in both laboratory and outdoor environments.

2. DESIGN SUMMARY

2.1 Sensor Layout

Figure 2a shows a solid model of the CS-HSI layout with the corresponding ray traces overlaid. The definitions for each component are included in the Figure. As described above, the incoming light from the sensor is spectrally encoded by the FPTF and is imaged onto the DMD. A total internal reflectance (TIR) prism is used to redirect the light from the DMD to the collimating lens while maintaining a compact footprint. The fold mirror allows for precise steering of the light through the exit optics and onto the PD. A spectral cold filter is included in the detector assembly to limit the background shot noise from 2-13 μm (the full range of the MCT PD) down to 8-10.4 μm (the required range for this application). This increases the D* of the detector by a factor of 1.7× resulting in a radiometric enhancement for the detector. The system model is further described in Section 2.2.

The sensor achieves 8-10.5 μm spectral range with 10 cm^{-1} spectral resolution provided by the FPTF. The optics support a field of view (FOV) of 18° circular with a corresponding instantaneous FOV (IFOV) of 2.5 mrad. The IFOV supports a spatial resolution of 7.5 m at a standoff of 3 km. The total radiometric efficiency of the CS-HSI including losses from the FPTF and DMD is 26%. Figure 2b shows a photograph of the CS-HSI sensor with the environmentally hardened lid removed to show the optical components of the sensor.

The sensor layout also includes a small LWIR microbolometer (not shown in Figure 2). The microbolometer is aligned with the CS-HSI to provide LWIR contextual imagery to accompany the hyperspectral data cubes. In addition to providing context to the overall scene, the LWIR images may also be used to inform or enhance the CS image reconstructions or ATR detection algorithms through a fusion effort.

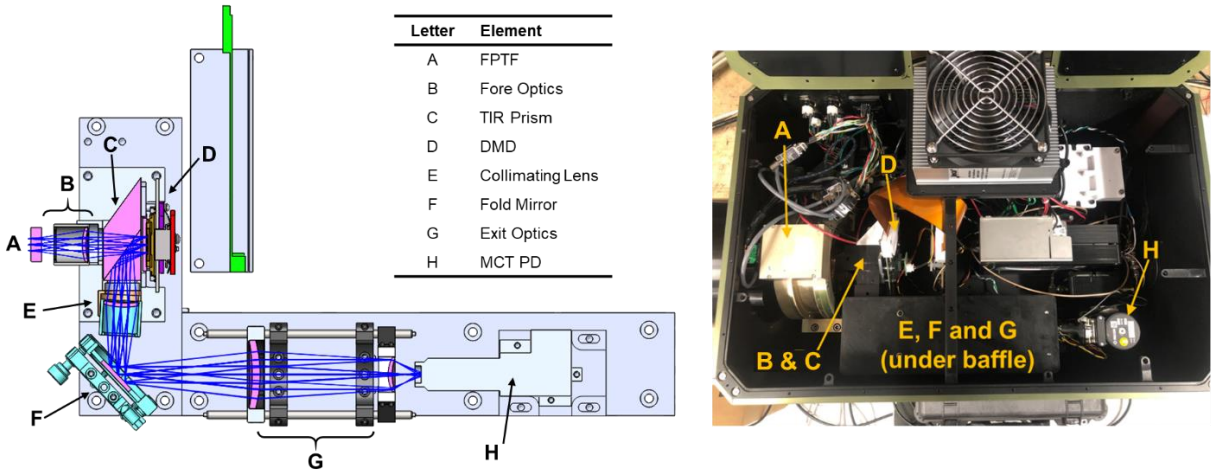

Figure 2. CS-HSI a) solid model with corresponding ray traces and b) photograph of the sensor. Definitions for each element are included in the Figure.

2.2 System Model

The purely radiometric system model predicts the CS-HSI's performance with regard to acquisition time and noise equivalent spectral radiance (NESR). The NESR determines the minimum detectable concentration pathlength product (CL_{min}) for a detector-noise limited system. NESR values are derived based on a constant false alarm rate signal to noise ratio (SNR) analysis assuming a 3 K temperature contrast between the plume and background. NESR and CL_{min} are given as:

$$\mathrm{NESR} = \frac{\sqrt{\mathrm{A_d}/N_{spat\_re}}}{\mathrm{D^*}\cdot\frac{\Theta}{N_{spat\_re}}\cdot\eta_{\mathrm{FPTF\_sys}}\cdot\eta_{\mathrm{spat\_m}}\cdot\Delta\sigma\cdot\sqrt{\Delta t_{FPTF}}}\ [=]\ \frac{\mathrm{W}}{\mathrm{cm^2\cdot ster\cdot cm^{-1}}} \tag{1}$$

and

$$\mathrm{CL_{min}} = -\frac{1}{\alpha}\cdot\ln\left(1-\frac{\mathrm{SNR_{discriminant}}\cdot\mathrm{NESR}}{\Delta\mathrm{N}}\right)[=]\ \mathrm{mg/m^2} \tag{2}$$

where α is the absorption cross section of the detected species and all other parameters are defined in Table 2.

Table 2. NESR parameters

Parameter	Description	Value	Units
A_d/N_{spat_re}	Detector area divided by the number of spatial resolution elements	$0.16/N_{spat\_re}$	cm^2
N_{spat_re}	Number of spatial resolution elements	64×64	unitless
D*	Detectivity (77 K MCT)	3.35×10^{10}	$cm\sqrt{Hz}/W$
Θ	Spatially integrated etendue	0.074	cm^2ster
η_{spat_m}	CS spatial mask efficiency	0.5	unitless
η_{FPTF_sys}	FPTF total system radiometric efficiency	0.26	unitless
Δσ	Spectral resolution	10	cm^{-1}
Δt_{FPTF}	FPTF integration time per spectral band [3]	Variable	s

The integration time is dictated by the sampling requirements where the effective integration time of the FPTF is given by:

$$\Delta t_{FPTF} = \frac{samp_{spat}\cdot N_{spat\_re}}{11{,}350}\ [=]\ s \tag{3}$$

11,350 Hz is half of the maximum binary frame rate allowed by the DMD corresponding to the maximum on-off modulation frequency for the WH masks that serve as the basis set for the CS. Figure 3a shows the total hyperspectral data cube integration time assuming the FPTF steps through 30 spectral bands. Figure 3b shows the predicted NESR as a function of sampling ratio based on a single integration time associated with the sampling ratio at each band. Figure 3c shows the predicted CL_{min} as a function of sampling ratio for four plume to background contrast values based on the known line strength of the 9.8 μm Sarin peak (α = 6×10^{-3} m^2/mg). The purely radiometric system is predicted to meet the threshold CL_{min} KPP for the 3 K temperature contrast with a sampling ratio of 0.35. The sensor is projected achieve the objective CL_{min} at larger temperature contrast (> 10 K) or at 3 K temperature contrast by coadding 50 hyperspectral cubes sampled at 0.35 ratio.

The model shows that the sensor will be able to reach the JSLSCAD threshold requirement of 135 mg/m^2 for a 3 K temperature contrast at sampling ratios up to 0.3 on a per-FOV basis. The CS-HSI meets the objective KPP of 135 mg/m^2 for a 10 K temperature contrast at a sampling ratio of 0.6 on a per-FOV basis.

Taking into account JSLSCAD field of regard and time to detect KPPs, the CS-HSI can dwell on each 18° FOV for 27 s and cover 60° in 90 s. At this effective integration time and based on a constant false alarm rate analysis, the CS-HSI is able to achieve 90% P_d with 3×10^{-4} probability of false alarm (P_{fa}) at 135 mg/m^2 and 3 K temperature contrast. The mean time between false alarms (MTBFA) associated with continuous operation and a 90 s time to detect is 83 hours.

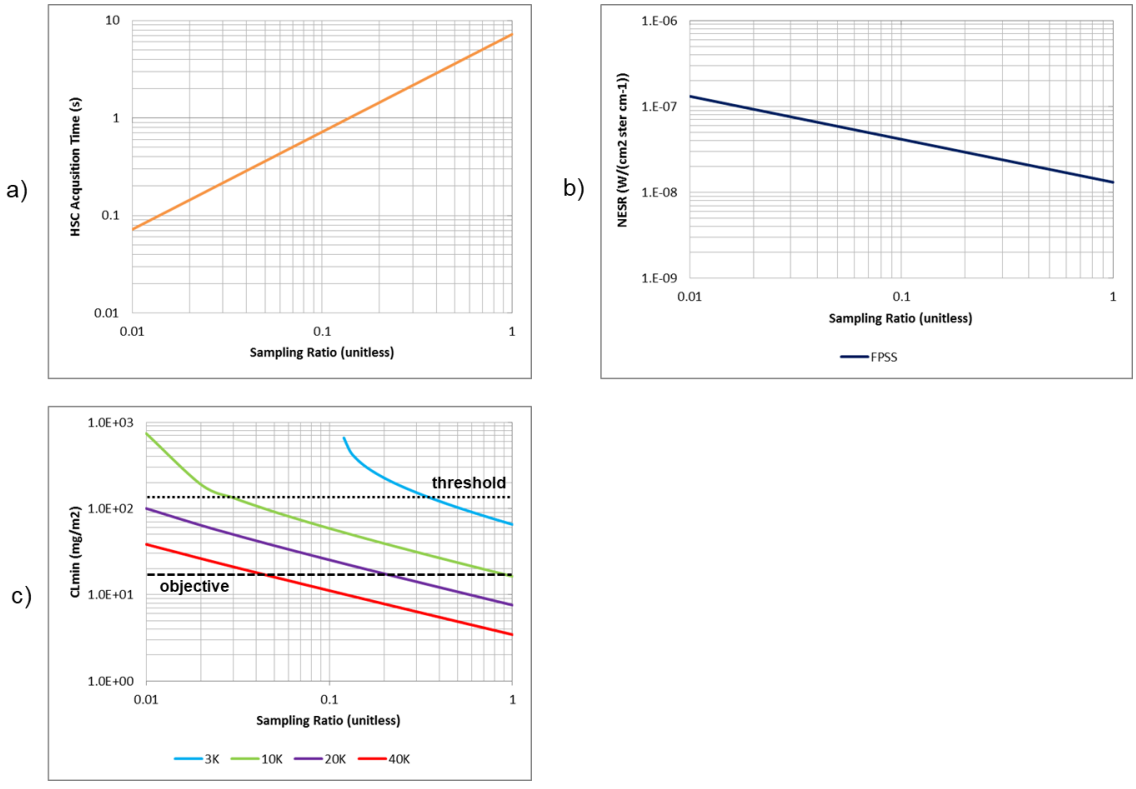

Figure 3. System model predictions of the a) hyperspectral data cube acquisition time as a function of sampling ratio, b) NESR as a function of sampling ratio and c) CL_{min} as a function of sampling ratio for several plume to background contrast values.

2.3 Sensor Hardening

In anticipation of field testing, the CS-HSI has been integrated into an environmentally hardened housing. Figure 4 shows photographs of the environmentally hardened CS-HSI. The FPTF is located in the black nose cone on the front of the sensor which has a conical internal angle of 18°, consistent with the 18° FOV of the sensor. This acts to reject ambient LWIR light while protecting the actuators of the FPTF. At the opening of the conical nose cap is a 3" ZnSe window that serves protect the CS-HSI sensor from the environment during field testing while still allowing for LWIR imaging.

The anodized aluminum housing contains the optics for the sensor, the MCT detector and pre-amp, and the data acquisition (DAQ) module. The housing has an external panel, which contains an on/off switch to power the sensor when connected to a 120V/60Hz wall outlet. Three main components can be turned on via LED push buttons on the panel – the USB hub, the DMD, and the cryocooler for the MCT detector. The upper left panel has connectors to communicate with the FPTF and the lower left panel has access to the USB hub as well as three auxiliary USB ports. The center right section of the control panel has indicator LEDs to alert the user for when the system and DAQ are powered and when the detector cryocooler is cold and ready. The control panel is IP65 compliant, implying complete protection from dust, oil, water spray.

The CS-HSI is cooled via a thermoelectric cooler (TEC) installed on the top of the housing. At an ambient temperature of 35°C, this TEC is capable of removing 37 W of power (i.e. the CS-HSI power draw) from system and maintaining an internal sensor temperature of 25°C. This internal temperature is well within the thermal specifications of the components in the CS-HSI (maximum operating temperature of ~50°C) making it suitable for field demonstrations.

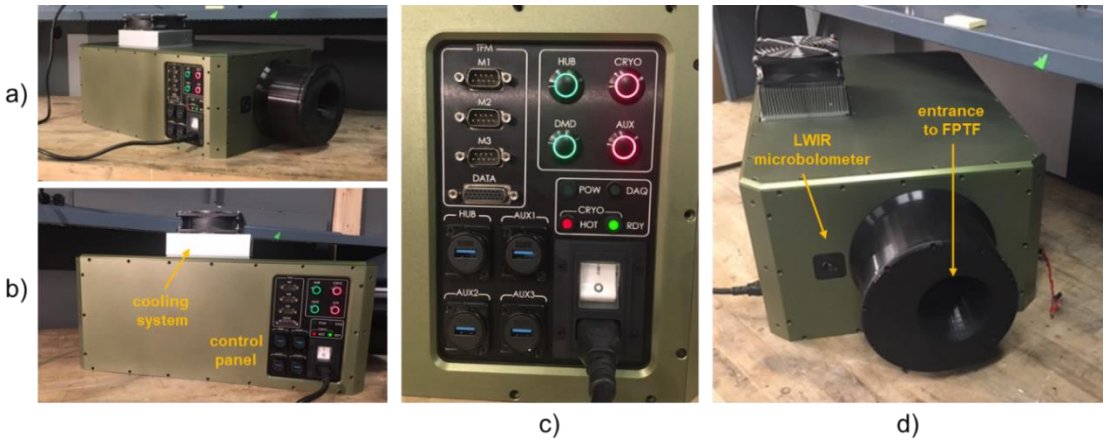

Figure 4. Photographs of the CS-HSI sensor integrated into the environmentally hardened housing, highlighting a) the entire sensor, b) the cooling system and control panel, c) a close-up of the external control panel, and d) the entrance to the FPTF and the LWIR context camera.

3. FUNCTIONAL TESTING

3.1 Spatial and Spectral Resolution

Spectral and spatial resolution was measured using the CS-HSI mounted to a tripod with tip-tilt-pan capabilities and set up to image an infragold plate against a 25°C blackbody. A tunable QCL was set to ~1200 cm^{-1} (1 cm^{-1} linewidth) and aimed at the infragold plate. Hyperspectral imagery was acquired from 1000-1250 cm^{-1} with 10 cm^{-1} wavelength steps of the FPTF using all 4096 WH masks at both the center and edge of the FOV, achieved by moving the CS-HSI location via the tripod. The dot products from the data acquisitions were reconstructed into hyperspectral data cubes through a full linear inversion (i.e. 0% compression). The method used to reconstruct the CS-HSI images is based on the L1 split Bregman iteration. [1-2] Figure 5 shows two such reconstructions where the QCL spot is seen as a dark blue feature and is highlighted with an arrow. 1D cuts were taken through the center of the QCL spots in the spectral

and spatial dimensions to determine the spectral and spatial resolution of the CS-HSI. The top plots in Figures 5a and 5b display the spatial resolution of the ~1200 cm^{-1} QCL which has an average FWHM of 14 cm^{-1}. The spatial resolution, shown in the bottom plots of Figures 5a and 5b is measured to be 0.58 pixels corresponding to an IFOV of 4.9 mrad. This spatial resolution is sufficient for plume detection and bearing, and is also compatible with the ability to reconstruct scenes with 128×128 spatial resolution elements with an IFOV of 2.5 mrad. These experiments show that the spectral resolution of the sensor is 14 cm^{-1} and the spatial resolution 4.9 mrad, in line with the KPPs of the CS-HSI.

a)

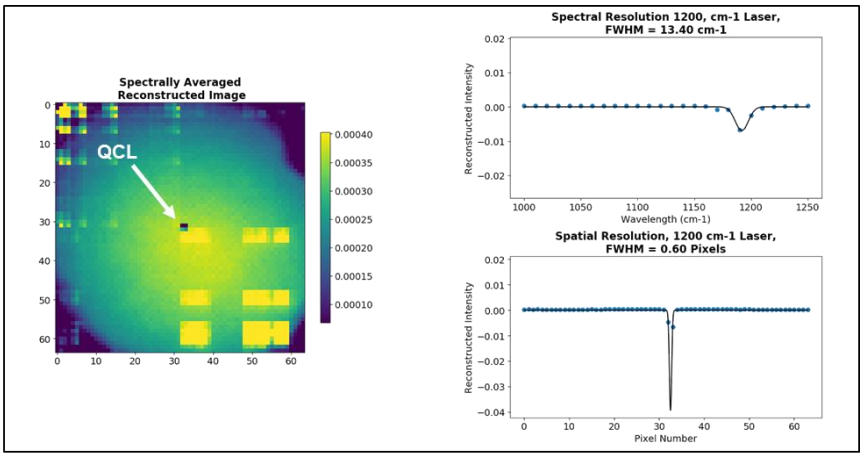

b)

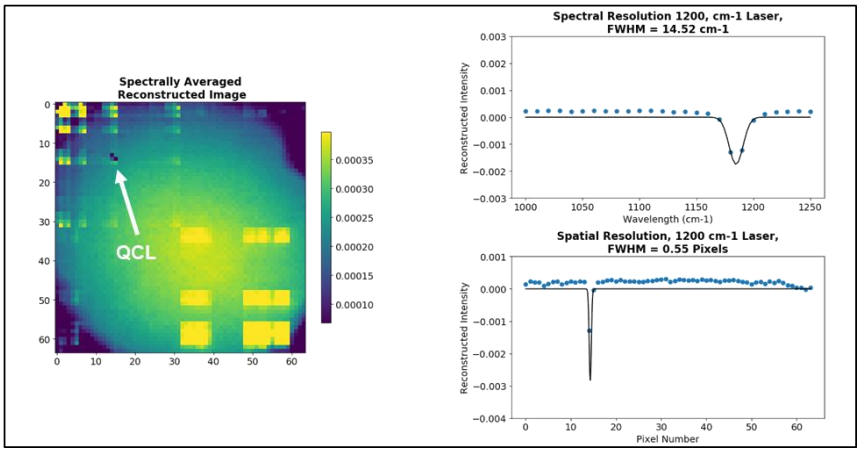

Figure 5. Spectrally averaged reconstructed hyperspectral data cubes, and spectral and spatial resolutions for a ~1200 cm^{1} QCL at the a) center and b) corner of the FOV.

3.2 NESR

The NESR predictions of the CS-HSI are described in Section 2.2. The NESR reported here is the spatially resolved NESR which is determined by imaging a blackbody at 20°C and 50°C such that the blackbody filled the FOV and the aperture of the CS HSI. The sensor was commanded to take two sequential images at each blackbody temperature by flipping through all 4096 WH masks for three wavelengths: 1050, 1150, and 1250 cm^{-1}. The NESR was then calculated by Equation 4, where Δ_{rad} is the change in radiance of the imaged blackbody at the two temperatures, σ_{img} is the spatial standard deviation of the difference of two sequential images divided by $\sqrt{2}$ (to compensate for the uncorrelated noise sources of the two images) and $img_{50/20C}$ is the spatially integrated image at either 50°C or 20°C.

$$NESR = \frac{\Delta_{rad} \times \sigma_{img}}{(img_{50C} - img_{20C})} \quad (4)$$

Figure 6 shows the spatially resolved NESR maps and corresponding histogram for the CS-HSI for various levels of compression at 1150 cm^{-1}. This shows that with 0% compression (100% sampling) the NESR is on the order of 1×10^{-6} $W/(cm^2\ sr\ cm^{-1})$. Figure 6 also shows that the as the level of compression increases, the NESR decreases. Therefore, for the 10% sampling, the corresponding NESR is 0.4 $\mu W/(cm^2\ sr\ cm^{-1})$, which is within a factor of 4 of the requisite NESR for the CS-HSI. Note that reconstructing the CS-HSI imagery with different levels of compression (that is, not just a linear inversion) can be done several ways based on which WH masks are used. As previously discussed, a key component for obtaining believable reconstructions from sampled data at 90% compression was to use a special ordering on the WH masks, which maximized the variance of the dot products across many training HSI data cubes (i.e. sequency ordering). [3-4] This sequency ordering is used throughout the rest of this study.

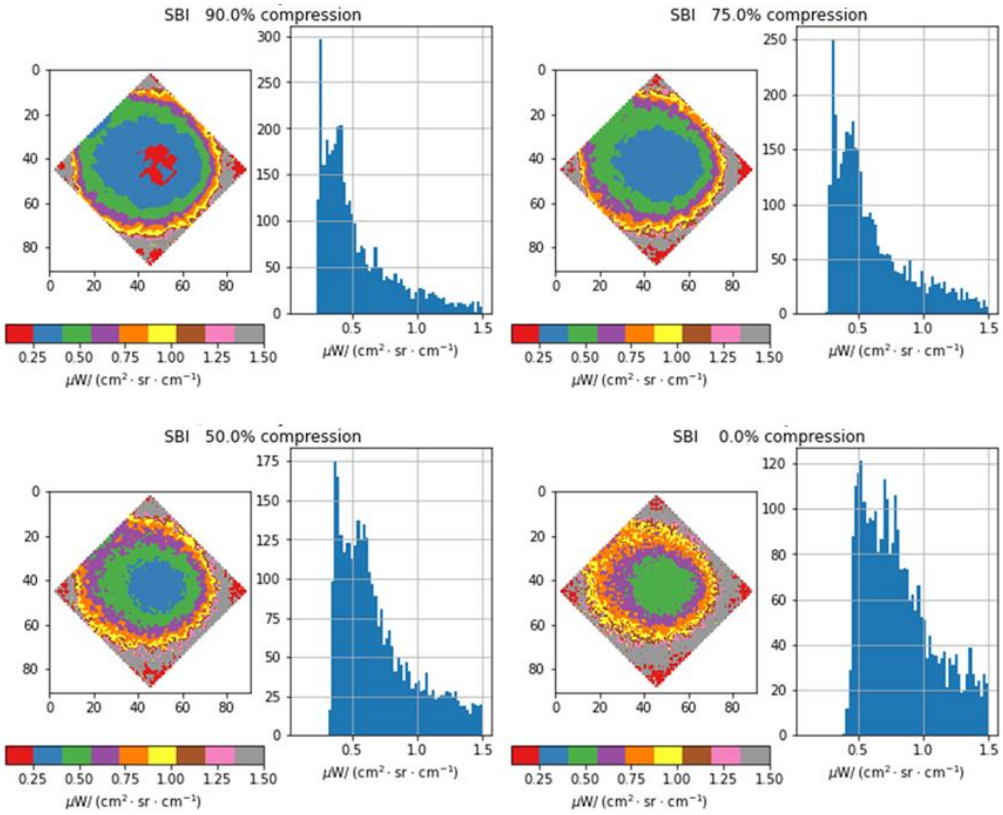

Figure 6. Spatially resolved NESR for the CS-HSI using an 11.3 kHz waveform and the inverse WH masks as the off mask for various levels of compression.

4. DEVELOPMENTAL TESTING

4.1 Laboratory Testing

The refrigerant R-134 was used during this effort as a simulant for the CS-HSI prototype. To validate the CS-HSI sensor and detection algorithms in a laboratory setting, the CS-HSI was set up to monitor a flow cell containing known concentrations of the simulant gas R-134. Figure 7a shows the sensor integrated with a tripod, and Figure 7b shows the flow cell arrangement. Here, a flow cell is created out of an infrared transmissive plastic and is attached to two gas tanks that can both be set to precise flow rates. One tank contains the simulant gas and the other contains pure nitrogen gas to control the concentration in the flow cell. The flow cell sits in front of a small blackbody, which was set to 70°C. Behind the small blackbody is a large blackbody that is set to 25°C to force contrast between the gas and the background. This mimics the scene that the CS-HSI monitors as a simulant is released against the cold sky. A reference window is created out of the same plastic as the flow cell so that the material of the flow cell can be subtracted out and only the response from the simulant remains.

Two different concentrations of R-134 were observed by the sensor, 4424 ppm and 8810 ppm. Figure 8 shows the background subtracted linear inversion reconstructions of R-134 in the flow cell at each wavelength interrogated by the CS-HSI for the 4424 ppm case where the background is taken from the region of the small blackbody behind the reference window. As the wavelengths approach 1170 cm^{-1}, a darker feature appears near the center of the image and is highlighted with an arrow in the Figure. This is where the flow cell is located and the wavelength where the dark feature appears is close to the main absorption feature of R-134A at 1190 cm^{-1}.

Figure 7. a) Photograph of the CS-HSI sensor integrated to a tripod to monitor b) the experimental setup containing the simulant R-134.

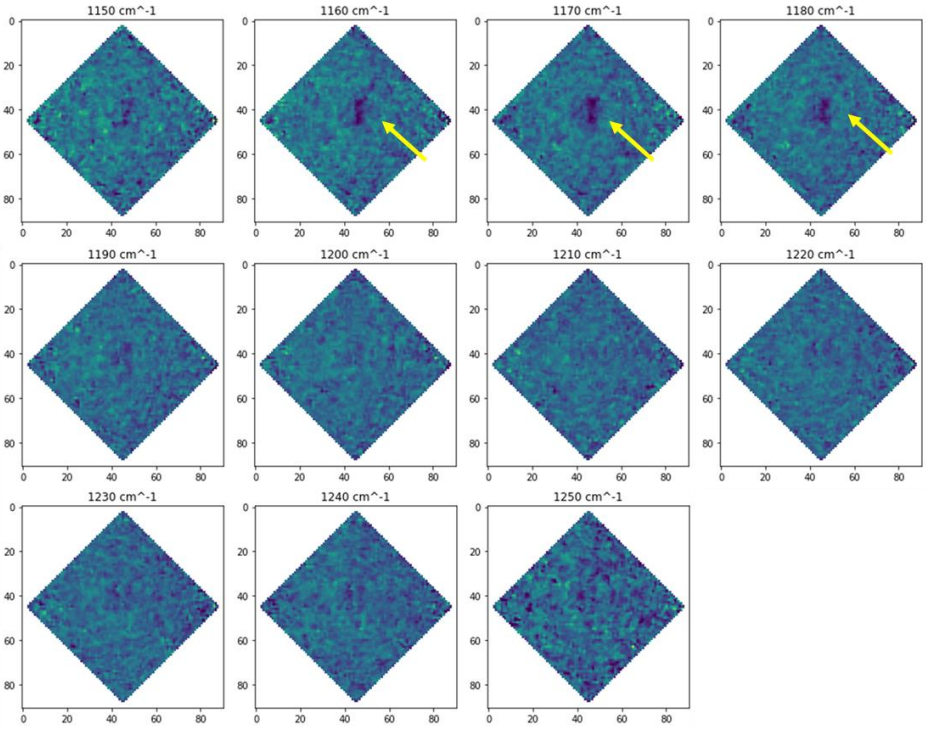

Figure 8. Linear inversion reconstructions of the flow cell containing R-134 for each wavelength interrogated by the CS-HSI.

If each linear inversion is stacked upon each other and a 1D cut is taken in the wavelength direction, the purple spectrum in Figure 9 is produced. Similarly, the red trace in Figure 9 is the 1D cut taken in the wavelength direction for the 8810 ppm concentration of R-134. The purple and red dashed spectra are the reference spectra of R-134 at these two different concentrations, which shows the absorption feature at 1190 cm^{-1}. Note that there is a shift of the absorption peak between the measured spectra and the reference spectrum of about 20 cm^{-1} to the red. This is due to a calibration error between the reference spectrum and the FTIR used to calibrate the FPTF, which can easily be recalibrated.

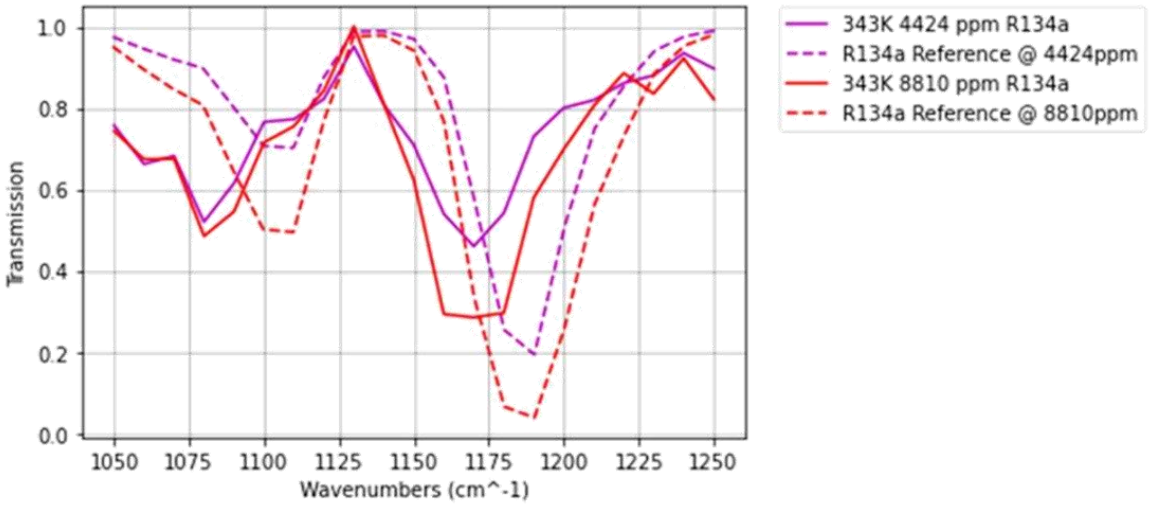

Figure 9. Transmission spectra of the two concentrations of R-134 acquired with the CS-HSI and the corresponding reference spectra.

The data collected during this effort was also used to investigate multi-resolution detection – that is, detection for a chemical signature in a scene at multiple scales, as seen in see Figure 10. [5] The upper left-hand image shows the reconstructed image under 10% sampling that has been integrated over all wavelengths. The top center image shows a detection map produced using traditional ACE where the yellow region implies detection of R-134. The top right image is the detection map produced using MVDR where once again the yellow region implies detection. The remaining detection maps were generated using MVDR in transform space (i.e. *from the dot product measurements with no reconstruction*) using different scales of the wavelet domain. Here, MVDR detection in transform space was revisited and the optimization problem was modified to reconstruct detection statistics rather than an image. [5] Figure 10 shows that this detection can be performed with the compressed data implying faster computation for detection. Furthermore, these detection maps show that the CS-HSI and algorithms are capable of detecting R-134 in a laboratory environment under 10% compression. This laboratory capability demonstration shows that the CS-HSI is capable of detecting 417 mg/m^2 of R-134 in a flow cell with 45 K temperature contrast with high (90%) compression.

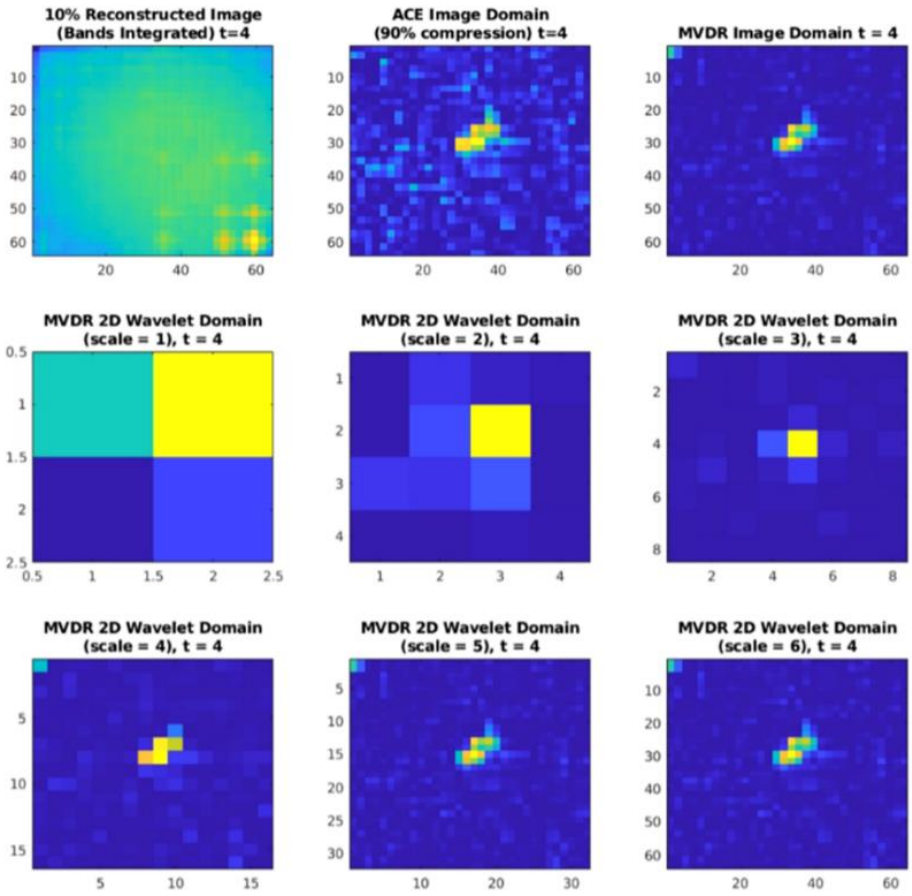

Figure 10. Detection maps of flow cell hyperspectral data cubes containing R-134 sampled with 10% of the WH masks in the sequency ordering where the MVDR in the transform domain at different scales in the 2D-Haar domain alongside an ACE detector.

4.2 Outdoor Testing

After validation of the CS-HSI sensor was performed in the laboratory, validation experiments were performed outside to measure a "plume" of R-134 in a more accurate operational environment. A chamber was placed on the roof of the main PSI office to contain the plume of R-134. The chamber was constructed out of a wooden frame and polyethylene, which is transmissive in the LWIR, and measured 17"×20" with a depth (or pathlength) of 4 cm. Note that this pathlength is extremely small with respect to operationally relevant chemical plumes, but the concentrations in this experiment are significantly higher than what would be observed in the field, and as such similar results (i.e. CL) are achieved. A reference window was located to the left of the gas chamber, containing two sheets of the polyethylene, similar to the laboratory experimental setup described in the previous subsection. The chamber also contained a sheet of polystyrene which has a distinct signature in the LWIR to serve as a secondary target to measure. The CS-HSI was placed on a tripod on the ground and tilted at an angle of 32° to monitor the chamber. Figures 11a and 11b show photographs of the sensor in this configuration as well as the ground control station.

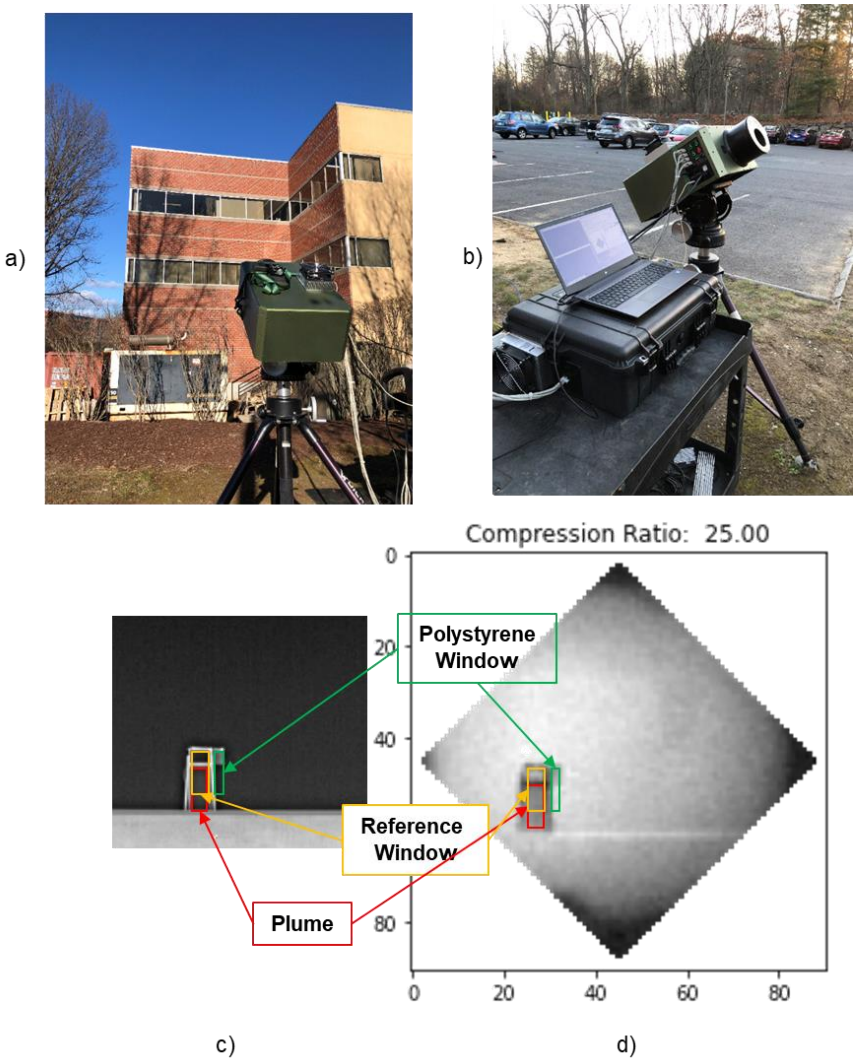

Figure 11. Photographs of the outdoor experimental setup of the CS-HSI showing a) the look angle to the roof where the gas cell was located and b) the ground station for controlling the sensor.

Before each set of outdoor plume data was collected, the chamber was filled with R-134, and a spectral signature was acquired using a benchtop FTIR spectrometer. The FTIR measurements confirmed that the concentration of R-134 was 21,000 ppm. This corresponds to a CL of 3500 mg/m^2. Ambient temperatures hovered around 0° C (273 K) during this experiment and the temperature of the sky was assumed to be 250 K. To create greater contrast, an additional heating element was added to the chamber. With the heater running at about 70 W, the estimated temperature of the R-134 gas in the chamber was around 283 K corresponding to a contrast of 33 K. Each data cube was taken using all 4096 WH masks such that a subset of the masks could be selected to test the detection of the gas at different levels of compression in post-processing. Additionally, contextual LWIR images were obtained with the boresighted microbolometer. Figure 11c shows one such context image with the corresponding CS-HSI image with 25% compression shown in Figure 11d. In this LWIR context image, the R-134 gas chamber is clearly visible, along with the polyethylene reference window and the sheet of polystyrene, which also has a strong absorption in the LWIR.

Figure 12 shows the CS-HSI single pixel images reconstructed with compression ratios ranging from 25% to 98.4%. The red overlay in the images corresponds to detection made using the traditional ACE detection algorithms. This shows that detection of R-134 is achieved with extremely high compression ratios. In fact, localized R-134 was detected with compression up to 99.2% which corresponds to using only 16 WH masks. Figure 13 shows the extracted

spectra from these reconstructions in comparison to the reference R-134 spectrum. This shows that increased compression leads to decreased measured spectral modulation, which is what inhibits detections from being performed at even lower levels of compression. The detections observed during this experiment corresponds to a CL that is 12× higher than the threshold KPP for this application (135 mg/m^2 CL_{min} for Sarin at 3 K). However, the measured change in radiance for this detection is 2.7 μW/(cm^2 sr cm^{-1}) which is 8× higher than the NESR measured for the CS-HSI. This implies that lower concentrations of chemical agents can be measured with the CS-HSI, on a similar order of magnitude as the requisite KPP. Additional outdoor capability demonstrations were performed showing detection of 1335 mg/m^2 of R-134 with 37 K temperature contrast. However, these experiments were performed using suboptimal operating conditions that degrade the NESR of the sensor by a factor of 5×, which in concert predicts the ability to achieve the threshold detection limit with a 3K temperature contrast.

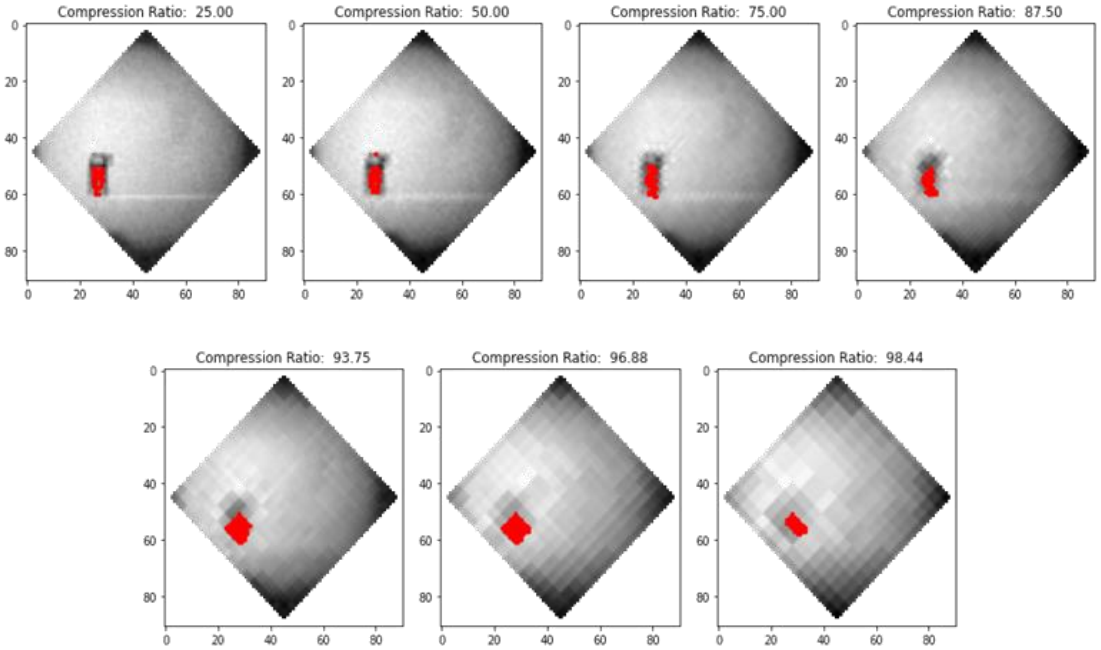

Figure 12. Detection maps for R-134 (red) at different levels of compression.

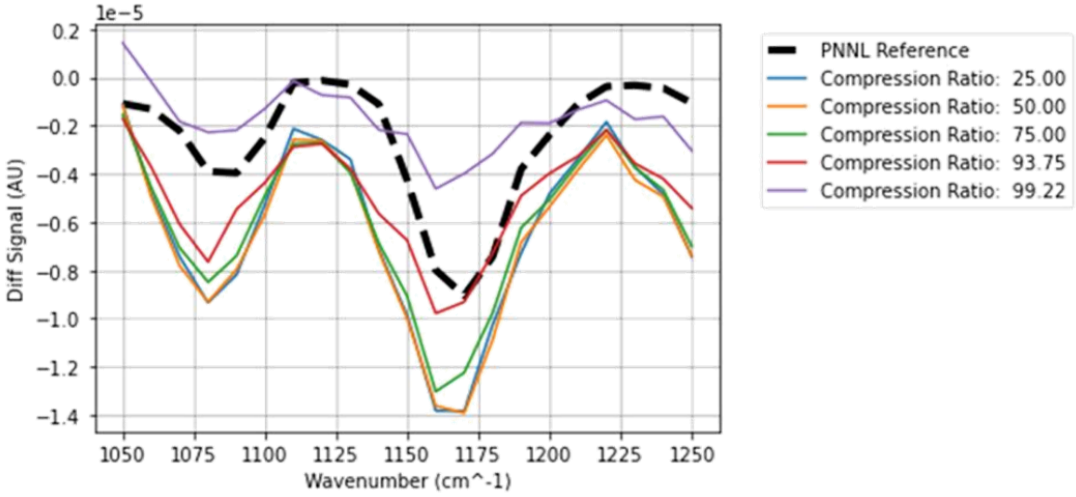

Figure 13. Extracted R-134 spectra at different compression levels and a reference R-134 spectrum.

5. CONCLUSIONS

A prototype CS-HSI sensor was designed, built, and validated against the KPPs through functional testing and capability demonstrations of chemical plume imaging in the LWIR in both laboratory and outdoor environments. This technology employed a FPTF to enable hyperspectral imaging, a DMD to spatially encode the image for CS, and compact and low-cost single pixel architecture. The sensor was ruggedized for operation in relevant environments.

The CS-HSI was designed to achieve a minimum detectable concentration pathlength of 135 mg/m^2 for 3 K temperature contrast over an 18° FOV with 2.5 mrad IFOV and 10 cm^{-1} spectral resolution. The prototype was used to demonstrate: acquisition of a 64×64×26 hyperspectral data cube over an 18° FOV with a 2.5 mrad IFOV; spatially resolved NESR of 4×10^{-7} W/(cm^2 sr cm^{-1}) for a 400 ms single wavelength acquisition time (assuming 10% sampling); and 13 cm^{-1} spectral resolution over 8-9.5 μm. A laboratory capability demonstration was performed showing the detection of 417 mg/m^2 R-134 in a flow cell with 45 K temperature contrast. Outdoor capability demonstrations were performed showing the detection of 1135 mg/m^2 and 3500 mg/m^2 of R-134 with 37 K and 33 K temperature contrast, respectively. When considering the change in radiance measured with respect to the achievable NESR, a factor of 5× and 8×, respectively, can be applied to the detected CLs to account for the full performance of the sensor, implying that the measured CL_{min} of the CS-HSI is closer to 227 mg/m^2 and 437 mg/m^2. The validated system model predicts the ability to achieve the threshold detection limit with a 3 K temperature contrast by retrofitting an AR coated ZnSe window on the DMD, achieving a radiometric efficiency of 2×.

ACKNOWLEDGEMENTS

This work has been supported by the U.S. Army, contract W911SR-19-C-0029. This support does not constitute an expressed or implied endorsement on the part of the Government.

REFERENCES

[1] Dupuis, J. R., Dixon, J. P., Schundler, E., Buchanan, S. C., Rameau, J. D., Mansur, D., Kvinge, H., Farnell, E., Peterson, C., and Kirby, M., "LWIR compressive sensing hyperspectral sensor for chemical plume imaging", Proc. of SPIE, 1141606-1, (2020).

[2] Joint Project Manager for NBC Contamination Avoidance Performance Specification for Commercial JSLSCAD document.

[3] Farnell, E., Kvinge, H., Dixon, J. P., Dupuis, J. R., Kirby, M., Peterson, C., Schundler, E. C., and Smith, C. W., "A data-driven approach to sampling matrix selection for compressive sensing", Proc. of SPIE, 1139603-1, (2020).

[4] Kvinge, H., Farnell, E., Dupuis, J. R., Kirby, M., Peterson, C., and Schundler, E. C., "More chemical detection through less sampling: amplifying chemical signals in hyperspectral data cubes through compressive sensing", Proc. of SPIE, 113920N-1, (2020).

[5] Kehoe, E. R., Kirby, M. M., Peterson, C., Scharf, L., Dupuis, J. R., Dixon, J. D., Anguita, M. R., and Craig, S. M., "Estimating chemical concentrations from compressed hyperspectral images", *Proc. of SPIE Submission*, (pre-print).